Complex Hyperfine Structure in the EPR Spectrum of $(FeF_6)^{3-}$ in CdTe†

L. C. KRAVITZ AND W. W. PIPER
General Electric Research and Development Center, Schenectady, New York
(Received 18 October 1965; revised manuscript received 20 December 1965)

The EPR and F^{19} electron-nuclear double resonance (ENDOR) of an $(FeF_6)^{3-}$-associated defect in CdTe have been studied. Very well resolved F^{19} hyperfine structure is observed and analyzed in terms of multiple reorientations of F^{19} nuclei. Splittings of the F^{19} ENDOR transitions are interpreted as nuclear spin-spin multiplet structure. The positions and intensities of all observed EPR transitions are in excellent agreement with the calculations. A theory of the ENDOR line splittings is presented which accounts for the observed nuclear multiplet structure including the enhancement of the ENDOR line splittings by the cubic crystalline fields. The hyperfine structure due to Fe^{57} has also been observed. The experimentally determined parameters are $S=\frac{5}{2}$, $g=2.0029$, $T_1^{19}=(+35.50\pm0.02)\times10^{-4}$ cm^{-1}, $T_2^{19}=(+14.66\pm0.02)\times10^{-4}$ cm^{-1}, $a=(+99.28\pm0.05)\times10^{-4}$ cm^{-1}, and $|A^{57}|=10.7\times10^{-4}$ cm^{-1}.

I. INTRODUCTION

THE EPR detection of isolated paramagnetic defects in II–VI semiconducting compounds has so far been limited to transition-metal and rare-earth ions, and centers thought to consist of chemical impurities associated with zinc and cadmium vacancies.[1] The observation of isolated shallow donors in n-type crystals appears to be prevented by impurity banding in presently available materials.[2]

In this paper we wish to report on a defect in CdTe which is created when fluorine, diffusing into single-crystal material containing trace amounts of iron, associates with the iron to form octahedrally coordinated paramagnetic FeF_6 complexes in the cubic zinc-blende lattice. The EPR spectra of these complexes exhibit extremely well-resolved F^{19} hyperfine structure and provide an exceptionally clean-cut example of the phenomenon of multiple nuclear transitions in EPR spectroscopy. A related problem concerning F^{19} hyperfine interactions of Mn^{2+} in ZnF_2 has received considerable study by Tinkham[3] and by Clogston *et al.*[4] The FeF_6 complex has been studied previously by Helmholz in K_2NaAlF_6 and by Hall *et al.* in $KMgF_3$ and $KCdF_3$.[5] The experimental conditions in these studies did not, however, justify a detailed analysis of the hyperfine structure such as that reported here.

II. EXPERIMENTAL TECHNIQUES

Single-crystal samples of CdTe were cleaved from ingots grown by zone-refining an ingot sealed in a quartz tube.[6] The samples were etched lightly, coated with a CdF_2 slurry, and air-dried at about 80°C. Thereafter the sample was sealed in an evacuated quartz vial and heated to 650°C for 24 h. One ingot was grown with the addition of 0.01% Fe (enriched to 80% Fe^{57}) to the charge.[7] Although none of the other crystals was intentionally doped with iron, all samples treated with CdF_2 produced the FeF_6 center.

Thermoelectric-probe measurements showed all of the fluorine-doped samples to be p-type, including those which were n-type before firing.

The EPR and electron nuclear double-resonance (ENDOR) measurements were carried out at 20.4 and 1.3°K using a 14-kMc/sec spectrometer, which has been described previously.[8] One additional measurement was made at 20.5 kMc/sec.

III. EPR RESULTS AND ANALYSIS

A. H Parallel to [100]

The resonance spectrum shown in Fig. 1 is seen when the magnetic field is oriented along a cube axis. In this orientation five fine-structure lines are observed, each of which is split into 15 resolved hyperfine lines. An examination of these fine-structure lines reveals that they each consist of three groups of five lines each. The groups have relative intensities 1:2:1 and the five lines within each group have relative intensities 1:4:6:4:1.

The entire spectrum of lines can be described by the Hamiltonian[9]

$$\mathcal{H}=g\beta\mathbf{S}\cdot\mathbf{H}+\tfrac{1}{6}a[S_x^4+S_y^4+S_z^4-\tfrac{1}{5}S(S+1)(3S^2+3S-1)]+\sum_{i=1}^{6}\{\mathbf{S}\cdot\mathbf{T}_i\cdot\mathbf{I}_i-\gamma_F\beta_N\mathbf{I}_i\cdot\mathbf{H}\}, \quad (1)$$

where the first and second terms are, respectively, the Zeeman and cubic field energies of the electronic spin

† Supported in part by the Aeronautical Research Laboratories, Office of Aerospace Research, U. S. Air Force.

[1] See review article by R. S. Title, in *II–VI Compounds*, edited by M. Aven and J. S. Prener (North-Holland Publishing Company, Amsterdam, to be published).

[2] K. A. Muller and J. Schneider, Phys. Letters **4**, 288 (1963).

[3] M. Tinkham, Proc. Roy. Soc. (London) **A236**, 549 (1956).

[4] A. M. Clogston, J. P. Gordon, V. Jaccarino, M. Peter, and L. R. Walker, Phys. Rev. **117**, 1222 (1960).

[5] L. Helmholz, J. Chem. Phys. **31**, 172 (1958); L. Helmholz and A. V. Guzzo, *ibid.* **32**, 302 (1960); T. P. P. Hall, W. Hayes, R. W. H. Stevenson, and J. W. Wilkins, *ibid.* **38**, 1977 (1963) and **39**, 35 (1963).

[6] M. R. Lorenz and R. E. Halsted, J. Electrochem. Soc. **110**, 343 (1963).

[7] We are indebted to H. D. Coghill for growing this ingot for us.

[8] G. W. Ludwig and H. H. Woodbury, Phys. Rev. **113**, 1014 (1959).

[9] See, for example, W. Low, in *Solid State Physics*, edited by F. Seitz and D. Turnbull (Academic Press Inc., New York, 1963), Suppl. 2, p. 114.

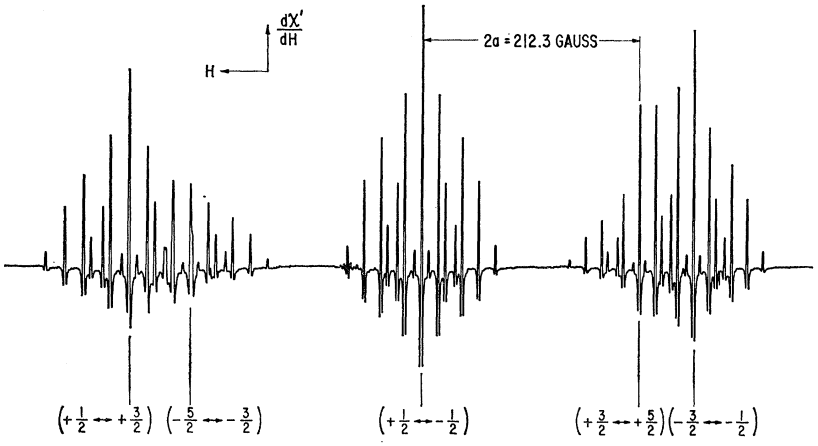

FIG. 1. Spectrum with H parallel to a [100] axis. $T=20.4°$K. Central line of each fine-structure set is marked. $\nu_e=14.2$ kMc/sec.

system and the last term is the interaction energy of the six F^{19} nuclear moments ($I=\frac{1}{2}$) with the electronic spin $S=\frac{5}{2}$ (Fe^{3+}) and with the external magnetic field H. The axis of the axially symmetric hyperfine tensors, $\mathbf{T}_i$, is the $[100]_i$ direction connecting the Fe ion with the ith F^{19} nuclear moment (see Fig. 2).

For H along a $[100]_{1,2}$ direction the energy levels given by Eq. (1) are[9]

$$W_{M,m_1\cdots m_6}=g\beta HM+C(M)$$
$$+M\left[T_1\sum_1^6 m_i+T_2\sum_3^6 m_i\right]-\gamma_F\beta_N H\sum_{i=1}^2 m_i \quad (2)$$

where M and m_i are the electronic and nuclear quantum numbers and $C(M)$ is the electronic energy associated with the cubic-field term of Eq. (1). The observed transitions occur for $\Delta M=\pm1$ and are given by

$$h\nu_e=g\beta H+D(M\pm1,M)+T_1N_1+T_2N_2, \quad (3)$$

where

$$D(\tfrac{1}{2},-\tfrac{1}{2})=0,$$
$$D(\pm\tfrac{1}{2},\pm\tfrac{3}{2})=\pm(\tfrac{5}{2}a\mp\tfrac{5}{16}a^2/h\nu),$$
$$D(\pm\tfrac{3}{2},\pm\tfrac{5}{2})=\pm2a,$$

and

$$N_1=\sum_{i=1}^2 m_i, \quad N_2=\sum_{i=3}^6 m_i.$$

The experimentally determined parameters are

$$|g|=2.0029,$$
$$a=(+99.28\pm0.05)\times10^{-4}\ \text{cm}^{-1},$$
$$T_1=(+35.50\pm0.02)\times10^{-4}\ \text{cm}^{-1},$$
$$T_2=(+14.66\pm0.02)\times10^{-4}\ \text{cm}^{-1}.$$

The sign of a was determined by measurements of fine-structure-line intensities at 1.3°K. The positive signs of T_1 and T_2 were determined from the results of the next section where "forbidden" hyperfine transition intensities are shown to depend upon MT_1 and MT_2. Once M is known from the low-temperature measurements, the positive sign of T_1 and T_2 can be deduced.

Each hyperfine line within the group associated with one $M\rightarrow(M+1)$ fine-structure transition may be labeled (N_1,N_2). The intensity of the line (N_1,N_2) is proportional to the number of combinations of m_i which result in N_1 and N_2, and thus to the product B_1B_2 where B_1 and B_2 are the binomial coefficients

$$B_1=2!/(1-N_1)!(1+N_1)!,$$
and
$$B_2=4!/(2-N_2)!(2+N_2)!. \quad (4)$$

This intensity variation is clearly shown in Fig. 3.

B. H Parallel to [111]

A more complicated spectrum results for arbitrary orientations of the magnetic field. Portions of one spectrum which we have studied in some detail are shown in Figs. 4 and 5 for a spectrometer frequency of 14.2 kMc/sec and in Fig. 6 for a frequency of 20.5 kMc/sec. H was oriented parallel to a [111] axis and thus the angles between the magnetic field direction and the six hyperfine axes are all equal. While Eq. (3) predicts a seven-line hyperfine spectrum, it is seen from Figs. 4 and 6 that (a) more than seven lines are observed, and (b) the spectrum is dependent upon the microwave frequency employed. These additional lines

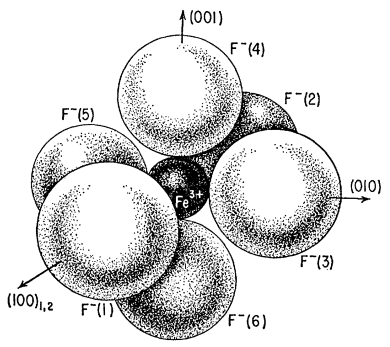

FIG. 2. A model of the $(FeF_6)^{3-}$ defect, as oriented in coordinates of the cubic zinc-blende lattice. The labeling of the F^{19} ions corresponds to that used in the text.

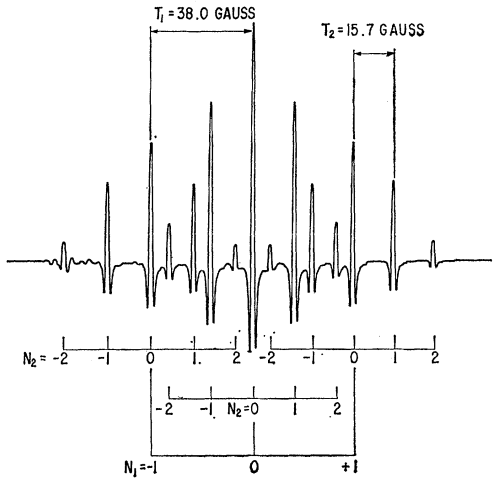

FIG. 3. The $(+\frac{1}{2}$ to $-\frac{1}{2})$ portion of the spectrum in Fig. 1. The hyperfine quantum numbers, N_1 and N_2, and the tensor components, T_1 and T_2, are indicated. $\nu_e = 14.2$ kMc/sec.

and their frequency dependence can be understood as electronic transitions for which the anisotropic F^{19} hyperfine interaction induces a simultaneous reorientation of one or more F^{19} nuclei. Such electron nuclear transitions have been discussed by Clogston *et al.*[4] who assumed that each F^{19} nuclear moment responds independently to the electronic transition. Following this approach we will first review the effect of a single nuclear spin on the EPR spectrum and then indicate the method employed to superimpose the effects of the six nuclear moments.

The Hamiltonian for a nuclear moment, interacting with an electronic spin and a magnetic field, can be written as in Eq. (1) as

$$\mathcal{H}_n = \mathbf{S}\cdot\mathbf{T}\cdot\mathbf{I} - \gamma_F\beta_N\mathbf{H}\cdot\mathbf{I}.$$

In what follows we assume that the electronic spin S is quantized along H with a quantum number M and that the nuclear states are quantized along the T_1 axis of the axial tensor $\mathbf{T}$. The contribution of $\mathcal{H}_n$ to the energy of the system is then given, to second order in the hyperfine interaction, by

$$E(M,m) = m\epsilon(M) = m(M/|M|) \times [(A-\nu)^2\cos^2\theta + (B-\nu)^2\sin^2\theta]^{1/2}, \quad (5)$$

where $m = \pm\frac{1}{2}$, θ is the angle between H and the axis T_1, $\nu = \gamma_F\beta_N H$, $A = MT_1 - T_2^2[S(S+1) - M^2]/2g\beta H$, and $B = MT_2 - T_1T_2[S(S+1) - M^2]/2g\beta H$.

The corresponding nuclear-spin functions are

$$\varphi(M,\tfrac{1}{2}) = \alpha\cos\delta_M - \beta\sin\delta_M, \quad (6a)$$

$$\varphi(M,-\tfrac{1}{2}) = \alpha\sin\delta_M + \beta\cos\delta_M, \quad (6b)$$

where $\tan\delta_M = -(A-\nu)\sin\theta/\{\epsilon(M) - (B-\nu)\cos\theta\}$ and α and β are the nuclear-spin basis functions.

The electron-nuclear wave function is

$$\Psi(M,m) = \psi(M)\varphi(M,m),$$

and the $M \leftrightarrow (M+1)$ transition probability is proportional to

$$|\langle\Psi(M,m)|S_x|\Psi(M+1,m')\rangle|^2 = \tfrac{1}{4}[S(S+1) - M(M+1)]|\langle\varphi(M,m)|\varphi(M+1,m')\rangle|^2.$$

Thus, for a given $M \leftrightarrow (M+1)$ fine-structure line the hyperfine-structure intensity may be proportional either to

$$p_M = |\langle\varphi(M,m)|\varphi(M+1,m)\rangle|^2 = \cos^2(\delta_M - \delta_{M+1}), \quad (7)$$

where $m' = m$, or to

$$q_M = |\langle\varphi(M,m)|\varphi(M+1,m')\rangle|^2 = \sin^2(\delta_M - \delta_{M+1}), \quad (8)$$

where $|m'-m| = 1$.

Combining Eqs. (5) and (1) we see that lines of strength p_M occur at

$$h\nu_e = g\beta H + D(M+1,M) \pm \tfrac{1}{2}(\epsilon^+ - \epsilon), \quad (9)$$

where $\epsilon^+ = \epsilon(M+1)$ and $\epsilon = \epsilon(M)$. Additional lines of strength q_M occur at

$$h\nu_e = g\beta H + D(M+1,M) \pm \tfrac{1}{2}(\epsilon^+ + \epsilon). \quad (10)$$

$D(M+1,M)$ is a function of magnetic-field orientation.[9]

It will be convenient in making the extension from a single interacting nuclear moment to the case of several nuclear moments to characterize the hyperfine-line positions and intensities of the $M \leftrightarrow (M+1)$ electronic transition by the algebraic expression

$$\Phi(M) = pX\left(\frac{\epsilon^+ - \epsilon}{2}\right) + qX\left(\frac{\epsilon^+ + \epsilon}{2}\right) = pX(E) + qX(E+F), \quad (11)$$

where $X(y) = x^y + x^{-y}$, $2E = \epsilon^+ - \epsilon$, and $F = \epsilon$ and where the subscripts on p_M and q_M have been dropped. Equation (11) is a polynomial in x with each of the

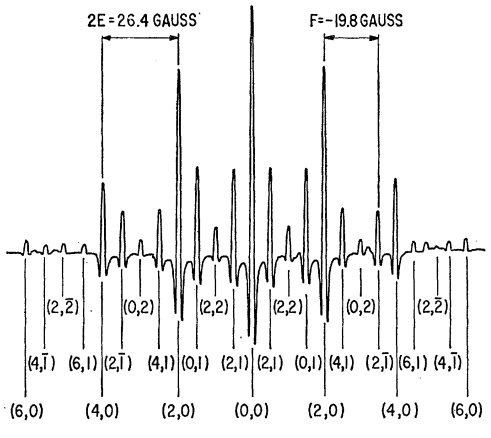

FIG. 4. $(+\frac{1}{2}$ to $-\frac{1}{2})$ transitions with H parallel to a [111] axis. Lines are labeled (j,k) [see Eq. (14) in text for definition]. All $(j,0)$ lines are the normally allowed transitions. Lines with $k \neq 0$ are so-called forbidden ("q" type) transitions. $\nu_e = 14.2$ kMc/sec.

TABLE I. Comparison of constants for observed line positions and line positions predicted from the [100] data. **H** is parallel to a [111] direction. Energies are in Mc/sec.

$(M+1) \leftrightarrow (M)$	$2E_{(calc)}$	$2E_{(obs)}$	$F_{(calc)}$	$F_{(obs)}$
A. Microwave frequency = 14.2 kMc/sec.				
$\frac{5}{2}, \frac{3}{2}$	71.32	71.4		
$\frac{3}{2}, \frac{1}{2}$	69.58	69.5	19.10	18.9
$\frac{1}{2}, -\frac{1}{2}$	74.35	74.1	−55.66	−55.5
$-\frac{1}{2}, -\frac{3}{2}$	70.49	70.3		
$-\frac{3}{2}, -\frac{5}{2}$	70.62	70.9		
B. Microwave frequency = 20.5 kMc/sec.				
$\frac{1}{2}, -\frac{1}{2}$	79.62	79.6	−64.39	−64.0

four terms corresponding to one of the resonances given by Eqs. (9) and (10). The coefficient of each term is proportional to the transition intensity while the exponent gives the shift of the hyperfine line relative to the average position

$$h\nu = g\beta H + D(M+1,M).$$

The expression $\Phi(M)$ is useful in dealing with several nuclear moments, each of which may have a different hyperfine interaction with the electron spin and thus a different $\Phi_i(M)$.[10] The entire spectrum of possible hyperfine lines for n nuclear moments will then be contained in the expression $\Phi_1(M)\Phi_2(M)\cdots\Phi_n(M)$.

As an example, the hyperfine spectrum due to two equivalent nuclear moments is given by

$$\Phi_1(M)\Phi_2(M) = (p^2+q^2)X(0)+2pqX(2E+F) +2pqX(F)+p^2X(2E)+q^2X(2E+2F).$$

Each value of the argument of X specifies the positions of a pair of symmetric lines and the coefficient of the term is proportional to the line intensity. When

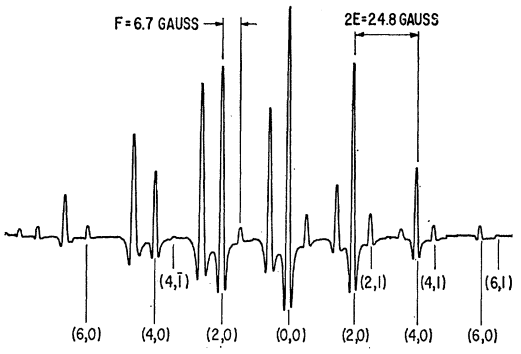

FIG. 5. ($+\frac{1}{2}$ to $+\frac{3}{2}$) and ($-\frac{5}{2}$ to $-\frac{3}{2}$) transitions with H parallel to a [111] axis. Only ($\frac{1}{2}$ to $\frac{3}{2}$) undergo q-type transitions and are labeled (j,k). Other q-type transitions ($k \neq 0$) lie under lines belonging to the ($-\frac{3}{2}$ to $-\frac{5}{2}$) set and are not marked. $\nu_e = 14.2$ kMc/sec.

[10] An equivalent formulation of this problem has been given recently by R. Lefebvre and J. Macuari, J. Chem. Phys. 42, 1480 (1965).

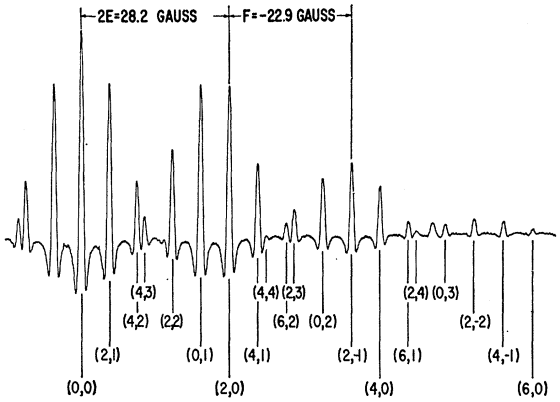

FIG. 6. The same transitions shown in Fig. 4 except that $\nu_e = 20.5$ kMc/sec.

$p=1$, $q=0$ ($\Delta m = \pm 1$ forbidden), the expression reduces to

$$\Phi_1(M)\Phi_2(M) = X(0)+X(2E) = x^{(\epsilon^+-\epsilon)}+2x+x^{-(\epsilon^+-\epsilon)},$$

which represents three hyperfine lines of intensity 1:2:1 equally spaced by $2E = \epsilon^+ - \epsilon$.

The extension of this technique to the case of $(FeF_6)^{3-}$, which has six equivalent F^{19} nuclear moments when H is parallel to the (111) axis, is made by evaluating the polynomial

$$\prod_{i=1}^{6} \Phi_i(M) = \sum_{j,k=1}^{6} C_{j,k}(p)X(jE+kF). \qquad (12)$$

The lines in Figs. 4 and 5 and Table II are identified by (j,k) corresponding to these indices in Eq. (12). Using $\nu_F = 4.0061$ Mc/sec·kG for F^{19} and values of T_1 and T_2 measured with **H** parallel to [100], the values of p, q, ϵ^+, and ϵ were computed from Eqs. (5), (6b), (7), and (8) and used to evaluate $C_{j,k}(p)$ and the arguments of X in Eq. (12). All of these computations were carried out with the aid of a GE 235 computer.

The excellent agreement between the calculated and experimental line positions and intensities, shown in Tables I and II, confirms the adequacy of the defect model and identifies the interacting nuclei as F^{19} independently of the ENDOR results. To demonstrate this latter point we have calculated the values of $2E$, F, and p for the $M=\frac{1}{2}$ to $M=-\frac{1}{2}$ electronic tranitions at 14.2 kMc/sec assuming that instead of F^{19} ($\nu_F = 4.0061$ Mc/sec·kG) the interacting nucleus was H^1 (4.2576 Mc/sec·kG). With this assumption the values of the parameters are changed as follows: $\Delta(2E) = 0.5$ Mc/sec, $\Delta F = 1.2$ Mc/sec, and $\Delta p = -0.02$. The sensitivity of the "q type" transitions ($\Delta m \neq 0$) to changes in p is such that for $\Delta p = -0.02$ the intensity of the (0,1) line increases from 0.346 to 0.406. It is thus clear from Tables I and II that the data are sufficiently precise to distinguish between F^{19} and the only other comparable nuclear moment H^1 and that only the F^{19}

TABLE II. Comparison of line intensities predicted from [100] data with integrated line intensities observed with **H** parallel to a [111] direction. Each set has been normalized to unity for the $(j,k)=(0,0)$ line. All (j,k) intensities for which $I_{(calc)}\geq 0.001$ are tabulated. The position of the (j,k) line relative to the central (0,0) line is given by $E(j,k)=(jE+kF)$ with the values of E and F shown in Table I in units of Mc/sec.

(j,k)	$\pm E(j,k)_{calc}$	I_{calc}	I_{obs}[a]
	A. $(M+1)\leftrightarrow M=(+\frac{1}{2}\leftrightarrow -\frac{1}{2})$		
	1. $\nu_e=14.2$ kMc/sec, $p=0.888$		
(0,0)	0.00	1.000	1.00
(4,3)	18.29	0.005 } 0.351	0.36
(2,1)	18.68	0.346	
(2,2)	36.97	0.064 } 0.106	0.10
(4,2)	37.36	0.042	
(0,1)	55.65	0.346 } 0.348	0.35
(6,3)	56.04	0.002	
(2,0)	74.33	0.739	0.74
(2,3)	92.62	0.005 } 0.175	0.18
(4,1)	93.01	0.170	
(0,2)	111.30	0.042 } 0.052	0.05
(6,2)	111.69	0.010	
(2,−1)	129.98	0.170	0.17
(4,0)	148.66	0.283	0.30
(0,3)	166.95	0.002 } 0.035	0.04
(6,1)	167.34	0.033	
(2,−2)	185.63	0.010	0.01
(4,−1)	204.31	0.033	0.04
(6,0)	222.99	0.044	0.05
	2. $\nu_e=20.5$ kMc/sec, $p=0.675$		
(0,0)	0.00	1.00	1.00
(2,1)	15.23	0.705	0.74
(6,4)	18.70	0.011	[b]
(4,2)	30.46	0.239	0.27
(4,3)	33.93	0.104	0.12
(6,3)	45.69	0.031	[b]
(2,2)	49.16	0.384	0.42
(0,1)	64.39	0.705	0.73
(2,0)	79.62	0.665	0.72
(4,1)	94.85	0.295	0.35
(4,4)	98.32	0.024	0.01_5
(6,2)	110.08	0.049	0.06
(2,3)	113.55	0.104	0.12
(0,2)	128.78	0.239	0.27
(2,−1)	144.01	0.295	0.34
(4,0)	159.24	0.181	0.23
(6,1)	174.47	0.040	0.06
(2,4)	177.94	0.011	0.01_5
(0,3)	193.17	0.031	0.04
(2,−2)	208.40	0.049	0.06
(4,−1)	223.63	0.040	0.05
(6,0)	238.86	0.014	0.02
	B. $(M+1)\leftrightarrow M=(\frac{3}{2}\leftrightarrow \frac{1}{2})$ $\nu_e=14.2$ kMc/sec, $p=0.963$		
(0,0)	0.00	1.000	1.00
(0,1)	19.10	0.114	0.11
(2,−1)	50.46	0.057	0.06
(2,0)	69.56	0.749	0.75
(2,1)	88.66	0.114	0.11
(4,−1)	120.02	0.011	0.01
(4,0)	139.12	0.298	0.30
(4,1)	158.22	0.057	0.06
(6,0)	208.68	0.049	0.06
(6,1)	227.78	0.011	0.01

[a] Time constant of recorded signal at 20.5 kMc/sec depressed larger signals disproportionately.
[b] Line is completely or partially unresolved from a strong neighboring line.

nuclear moment gives results in good agreement with the EPR observations.

The EPR spectrum of a CdTe sample containing 0.01% Fe^{57} (80% enriched) consists of three component spectra, each of which are identical to that of Fig. 1. Two displaced components result from the hyperfine splitting of the 80% abundant Fe^{57} ($I^{57}=\frac{1}{2}$), while a third central component is due to the other Fe isotopes ($I=0$). The two displaced-component spectra are described by adding to Eq. (2) a term

$$3\mathcal{C}_n{}^{57}=A^{57}\mathbf{I}^{57}\cdot\mathbf{S},$$

where $|A^{57}|=10.7\times10^{-4}$ cm^{-1}, $I^{57}=\frac{1}{2}$.

IV. F^{19} ENDOR ANALYSIS

ENDOR measurements[11] were performed by partially saturating the central hyperfine line of the $(\frac{1}{2}\leftrightarrow-\frac{1}{2})$ fine-structure transition and simultaneously exposing the sample to rf magnetic fields in the frequency range of 40 to 50 Mc/sec. The change in intensity of the EPR signal due to F^{19} transitions between nuclear states resulted in the ENDOR signal shown in Fig. 7 for H parallel to the [100] direction.

The splitting of the ENDOR lines of Fig. 7 is thought to arise from an indirect nuclear-nuclear magnetic interaction, somewhat similar to that observed in high-resolution NMR spectroscopy.[12] This interaction lifts the degeneracy of the energy levels of equivalent nuclei, such as, for example, the four F^{19} nuclei labeled F(3), F(4), F(5), and F(6) in Fig. 2, which are equivalent when H is parallel to (100). Multiplet structure[13] is then observed since the energy required for the transition of any one of these four nuclear moments will depend upon the orientations of the others to which it is coupled.

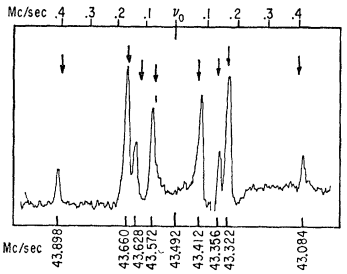

FIG. 7. ENDOR spectrum of the (0,0) EPR transition of Fig. 3. $\nu_e=14.05$ kMc/sec. $T=1.3$°K. The arrows indicate the line positions calculated by Eq. (14) and shown in Fig. 8.

[11] G. Feher, Phys. Rev. **114**, 1219 (1959).
[12] J. A. Pople, W. G. Schneider, and H. J. Bernstein, *High Resolution NMR* (McGraw-Hill Book Company, Inc., New York, 1959).
[13] A previous observation of structure in F center ENDOR has been reported by W. C. Holton, H. Blum, and C. P. Slichter, Phys. Rev. Letters **5**, 197 (1960). The analysis given in W. C. Holton and H. Blum, Phys. Rev. **125**, 89 (1962), neglects the hyperfine anisotropy and therefore does not reveal all of the structure reported here. An ENDOR analysis which includes hyperfine anisotropy and quadrupole effects of nuclear pairs is given in T. E. Feuchtwang, Phys. Rev. **126**, 1628 (1962). We wish to thank Professor Slichter for calling our attention to this latter reference.

TABLE III. Zero-order spin functions for equivalent nuclei F(3), F(4), F(5), and F(6) in permutation group symmetry D_{4h}.

$^5(A_{1g})_2$	$\alpha\alpha\alpha\alpha$
$^5(A_{1g})_1$	$\frac{1}{2}(\alpha\alpha\alpha\beta+\alpha\alpha\beta\alpha+\alpha\beta\alpha\alpha+\beta\alpha\alpha\alpha)$
$^5(A_{1g})_0$	$(1/\sqrt{6})(\alpha\alpha\beta\beta+\alpha\beta\beta\alpha+\beta\alpha\alpha\beta+\beta\beta\alpha\alpha+\alpha\beta\alpha\beta+\beta\alpha\beta\alpha)$
$^5(A_{1g})_{-1}$	$\frac{1}{2}(\beta\beta\beta\alpha+\beta\beta\alpha\beta+\beta\alpha\beta\beta+\alpha\beta\beta\beta)$
$^5(A_{1g})_{-2}$	$\beta\beta\beta\beta$
$^3(B_{2g})_1$	$\frac{1}{2}(\alpha\alpha\alpha\beta-\alpha\alpha\beta\alpha+\alpha\beta\alpha\alpha-\beta\alpha\alpha\alpha)$
$^3(B_{2g})_0$	$(1/\sqrt{2})(\alpha\beta\alpha\beta-\beta\alpha\beta\alpha)$
$^3(B_{2g})_{-1}$	$\frac{1}{2}(\beta\beta\beta\alpha-\beta\beta\alpha\beta+\beta\alpha\beta\beta-\alpha\beta\beta\beta)$
$^3(E_u)_1$	$(1/\sqrt{2})(\alpha\alpha\alpha\beta-\alpha\beta\alpha\alpha)$; $(1/\sqrt{2})(\alpha\alpha\beta\alpha-\beta\alpha\alpha\alpha)$
$^3(E_u)_0$	$(1/\sqrt{2})(\alpha\alpha\beta\beta-\beta\beta\alpha\alpha)$; $(1/\sqrt{2})(\alpha\beta\beta\alpha-\beta\alpha\alpha\beta)$
$^3(E_u)_{-1}$	$(1/\sqrt{2})(\beta\beta\beta\alpha-\beta\alpha\beta\beta)$; $(1/\sqrt{2})(\beta\beta\alpha\beta-\alpha\beta\beta\beta)$
$^1(A_{1g})_0$	$(1/\sqrt{12})(\alpha\alpha\beta\beta+\alpha\beta\beta\alpha+\beta\alpha\alpha\beta+\beta\beta\alpha\alpha-2\alpha\beta\alpha\beta-2\beta\alpha\beta\alpha)$
$^1(B_{1g})_0$	$\frac{1}{2}(\alpha\alpha\beta\beta-\alpha\beta\beta\alpha-\beta\alpha\alpha\beta+\beta\beta\alpha\alpha)$

The energy levels of the system of six nuclear moments may be calculated, as shown in the Appendix, by applying second-order perturbation theory to the electronic operators in the Hamiltonian

$$\mathcal{H}=g\beta\mathbf{H}\cdot\mathbf{S}+\sum_{i=1}^{6}(\mathbf{S}\cdot\mathbf{T}_i\cdot\mathbf{I}_i-\gamma_N\beta_N\mathbf{H}\cdot\mathbf{I}_i). \quad (13)$$

The nuclear Hamiltonian which remains has the symmetry of point group D_{4h} with regard to the permutations of nuclear indices when H is parallel to [100]. It may therefore be conveniently treated using the nuclear-product wave functions shown in Table III, which comprise the irreducible representations of the permutation group D_{4h}. ENDOR transitions are allowed only between nuclear states of the same irreducible representations since the interaction of the nuclei with the oscillating rf fields is completely symmetric with regard to permutation of the nuclei.

As shown in the Appendix, two terms of the nuclear Hamiltonian are diagonal in the nuclear states of Table III. These terms are

$$\mathcal{H}_{n0}(M)=N_1\{T_1M-\gamma_F\beta_NH-\mu_-(M)T_2^2\}+N_2\{T_2M-\gamma_F\beta_NH-\mu_-(M)T_1T_2\},$$

and

$$\mathcal{H}_{n1}(M)=\mu_+(M)\{\tfrac{1}{2}(T_1^2+T_2^2)(U_{35}+U_{46})+T_2^2U_{12}+T_1T_2(U_{34}+U_{45}+U_{56}+U_{63})\}, \quad (14)$$

where

$$N_1=\sum_{i=1}^{2}I_{zi},\quad N_2=\sum_{j=3}^{6}I_{zj},\quad U_{ij}=I_i^+I_j^-+I_i^-I_j^+$$

and $\mu_\pm(M)$ are parameters which depend upon the state of the electronic system. For any electronic state M, $\mathcal{H}_{n0}$ represents the sum of individual nuclear energies, while $\mathcal{H}_{n1}$ represents the coupling of the various equivalent nuclei. These terms lead to the zero-order nuclear energy levels shown in Fig. 8 for the four nuclei in the (100) plane. Transitions between these energy levels result in eight ENDOR frequencies

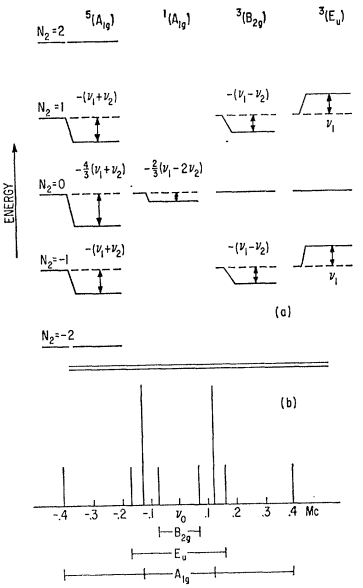

FIG. 8. (a) Energy levels of the nuclear Hamiltonian of Eq. (14) with $N_1=0$. The initial degeneracies of $\mathcal{H}_{n0}$ are shown split by $\mathcal{H}_{n1}$. (b) The theoretically calculated multiplet structure for transitions in which $\Delta N_1=0$, $\Delta N_2=\pm1$.

which are shown in Fig. 8:

$$\nu(A_{1g})=\nu_0\pm(\nu_1+\nu_2),\quad \nu_0\pm(\nu_1+\nu_2)/3;$$
$$\nu(B_{2g})=\nu_0\pm(\nu_1-\nu_2);$$
$$\nu(E_u)=\nu_0\pm\nu_1;$$

where

$$\nu_0=|MT_2-\gamma_F\beta_NH-\mu_-(M)T_1T_2|,$$
$$\nu_1=(\mu_+(M)/2)(T_1^2+T_2^2),$$

and

$$\nu_2=\mu_+(M)(2T_1T_2).$$

The ENDOR measurements shown in Fig. 7 were carried out on the $M=-\frac{1}{2}$ state for which

$$\mu_+(-\tfrac{1}{2})=-\frac{1}{4g\beta H}\left(1+20\frac{a}{g\beta H}\right),$$
$$\mu_-(-\tfrac{1}{2})=\frac{1}{4g\beta H}\left(17-20\frac{a}{g\beta H}\right).$$

Since $a/g\beta H=0.021$, the effect of the crystal field is to increase the multiplet splitting, proportional to $\mu_+(-\frac{1}{2})$, by about 28%.

The values of T_1, T_2, and $a/g\beta H$ determined in Sec. III, together with $M=-\frac{1}{2}$, and the F^{19} frequency, $\nu_F=4.0061$ Mc/sec·kG, give $\nu_0=43.44$ Mc/sec, as compared with the measured frequency $\nu_0=43.49$ Mc/sec. These same parameters give the multiplet spectrum shown in Fig. 8 and indicated by the arrows in Fig. 7. Thus the observed number and spacings of the ENDOR lines are very satisfactorily accounted for by the hyperfine interactions of four equivalent nuclear moments with an electronic moment of $S=\frac{5}{2}$ in a cubic crystalline field.

TABLE IV. Parameters of the EPR spectra of FeF_6 complexes. Units are 10^{-4} cm^{-1}.

	g	$\|a\|$	$\|A_s^{19}\|$	$\|A_p^{19}\|$
CdTe:Fe,F	2.0029	99.28±0.05	21.61±0.02	6.95±0.02
K_2NaAlF_6:Fe		58 ±2	22.4 ±0.5	6.5 ±0.5
$KMgF_3$:Fe	2.0031	51.2 ±0.5	24.0 ±0.5	6.0 ±0.5
$KCdF_3$:Fe	2.0027	53.0 ±2.0	22.6 ±0.5	5.6 ±0.5

V. DISCUSSION

The observed spectra have been interpreted in terms of the model shown in Fig. 2, although little direct evidence exists to suggest how the lattice accommodates this complex. Indirect evidence concerning the nature of the complex is available through a comparison of our measurements with those of Helmholz and of Hall *et al.*[5] on $(FeF_6)^{3-}$. The parameters to be compared are the F^{19} hyperfine coupling constants A_s which is related to the spin density of delocalized $3d$ electrons at the F^{19} nuclei, and A_p, which is related to the dipolar interaction between the unpaired electrons and the F^{19} nuclei. These parameters are listed in Table IV.

The apparent similarity between the value of A_s and A_p in these dissimilar materials strongly suggests that we are dealing with a $(FeF_6)^{3-}$ ion in CdTe. Two additional bits of evidence further suggest that this ion occupies a lattice site in which it does not covalently bond appreciably with the neighboring lattice atoms. First, the width (1.3 G) of the $M=\frac{1}{2}$ to $M=-\frac{1}{2}$ transition indicates very little hyperfine broadening due to the magnetic isotopes of neighboring Cd and Te ions. Second, the $M=\pm\frac{5}{2}$ to $M=\pm\frac{3}{2}$ transitions, which are sensitive to strain-induced variations in the cubic fine-structure parameter a, are almost as sharp as the $M=\frac{1}{2}$ to $M=-\frac{1}{2}$ transitions although the crystals probably are somewhat strained.

The size of the $(FeF_6)^{3-}$ complex is known for several inorganic fluorides in which the trivalent metal ion is surrounded by an octahedron of fluorine ions.[14] Available x-ray data give the average Fe-F distance in crystals isomorphic to $(NH_4)_3FeF_6$ as about 2.0 Å. More precise data are available for FeF_3 in which case the Fe^{3+} ion occupies a nearly octahedral site and Fe-F=1.94 Å. In the compound studied by Helmholz, K_2NaAlF_6, the trivalent Al occupies the octahedral site and Al-F=1.92 Å. It thus appears that a reasonable estimate for the Fe-F spacing in the FeF_6^{3-} ion for both K_2NaAlF_6 and CdTe is (1.95±0.05).

The lattice positions possessing the cubic symmetry required by the complex are the two interstitial sites as well as the Cd and Te sites. The two interstitial sites are both unlikely, due to their relatively small available volumes. The Te site provides a minimum of electrostatic energy for the trivalent negative ion as well as sufficient free volume for the $(FeF_6)^{3-}$ complex. Alternatively, since the Fe is incorporated into the lattice first, very likely at a Cd site, the $(FeF_6)^{3-}$ complexes may form by the diffusion of fluorine to the relatively immobile Fe. Sufficient free volume is available for the complex at a Cd site if the electronic charge on neighboring Te atoms takes the form of directed covalent bonds. The available evidence does not permit a clear choice between these two possibilities.

[14] R. W. G. Wykoff, *Crystal Structures* (Interscience Publishers, Inc., New York, 1948). See also L. Helmholz, A. V. Guzzo, and R. N. Sanders, J. Chem. Phys. 35, 1349 (1961).

ACKNOWLEDGMENTS

It is a pleasure to acknowledge the assistance of C. R. Trzaskos in performing the measurements, and of H. D. Coghill in supplying the CdTe starting material. We also wish to thank Dr. G. D. Watkins for recording the 20.5-kMc/sec spectra, Dr. F. S. Ham for critically reading the F^{19} ENDOR analysis, and Dr. F. H. Horn for making a crystal puller available to us. Helpful exchanges with Dr. J. S. Prener, Dr. G. A. Slack, and Dr. P. Pershan are also appreciated.

APPENDIX

Equation (14) may be derived by starting with Eq. (13) and setting

$$\mathbf{C}=\sum_{i=1}^{6}\mathbf{T}_i\cdot\mathbf{I}_i \quad \text{and} \quad \mathbf{F}=\sum_{i=1}^{6}\mathbf{I}_i.$$

Computing the electronic terms to second order in the hyperfine interaction gives

$$\mathcal{H}_n=C_zM-\gamma_N\beta_NHF_z+\tfrac{1}{2}\mu_+(M)(C^-C^++C^+C^-)+\tfrac{1}{2}\mu_-(M)(C^-C^+-C^+C^-),$$

where

$$\mu_\pm(M)=\frac{1}{4}\left\{\frac{\langle M|S^+S^-|M\rangle}{E_M-E_{M-1}}\pm\frac{\langle M|S^-S^+|M\rangle}{E_M-E_{M+1}}\right\},$$

$$C^\pm=C_x\pm iC_y, \quad \text{and} \quad S^\pm=S_x\pm iS_y.$$

With the magnetic field oriented parallel to [100], the matrix elements are, to first order in $a/g\beta H$, independent of the admixtures resulting from the crystal fields. The shifts of the energy levels do give measurable effects, however, and must be included in the energy denominators. Thus

$$E_M=g\beta HM+\epsilon(M),$$

where $\epsilon(\pm\frac{1}{2})=a$, $\epsilon(\pm\frac{3}{2})=-\frac{3}{2}a$, and $\epsilon(\pm\frac{5}{2})=a/2$. For H parallel to [100], the components of C are

$$C_x=T_1\{I_{3x}+I_{5x}\}+T_2\{I_{1x}+I_{2x}+I_{4x}+I_{6x}\},$$
$$C_y=T_1\{I_{4y}+I_{6y}\}+T_2\{I_{3y}+I_{5y}+I_{1y}+I_{2y}\},$$
$$C_z=T_1\{I_{1z}+I_{2z}\}+T_2\{I_{3z}+I_{5z}+I_{4z}+I_{6z}\}.$$

Using the commutation rules of angular momentum and the components of C, we find

$$C^-C^+-C^+C^-=-2\{T_2^2N_1+T_1T_2N_2\},$$
$$C^-C^++C^+C^-=2(C_x^2+C_y^2).$$

Expanding $C_x^2+C_y^2$, we find that

$$\mathcal{H}_n=\mathcal{H}_{n0}+\mathcal{H}_{n1}+\mathcal{H}_{n2}+\mathcal{H}_{n3}+\mathcal{H}_{n4},$$

where $\mathcal{H}_{n0}$ and $\mathcal{H}_{n1}$ are given in Eq. (14) and

$$\mathcal{H}_{n2}=\mu_+(M)(T_2(T_1+T_2)/2)\times(U_{13}+U_{14}+U_{15}+U_{16}+U_{23}+U_{24}+U_{25}+U_{26}),$$
$$\mathcal{H}_{n3}=\mu_+(M)((T_1^2-T_2^2)/2)\times\{(I_3^+I_5^++I_3^-I_5^-)-(I_4^+I_6^++I_4^-I_6^-)\},$$
$$\mathcal{H}_{n4}=\mu_+(M)(T_2(T_1-T_2)/2)\times\{(I_3^++I_5^+-I_4^+-I_6^+)(I_1^++I_2^+)+(I_3^-+I_5^-+I_4^--I_6^-)(I_1^-+I_2^-)\}.$$

The states which $\mathcal{H}_{n2}$, $\mathcal{H}_{n3}$, and $\mathcal{H}_{n4}$ connect have energy separations, due to $\mathcal{H}_{n0}$ and $\mathcal{H}_{n1}$, of 33, 84, and 117 Mc/sec, respectively. These operators therefore do not perturb the energy levels appreciably.

One complication arises due to the matrix element

$$\langle{}^5(A_{1g})_0|\mathcal{H}_{n1}|{}^1(A_{1g})_0\rangle=(\mu_+(M)/3\sqrt{2})(T_1-T_2)^2.$$

In principle, such a matrix element requires a diagonalization of the two initially degenerate $(A_{1g})_0$ states. In the present case, this matrix element is sufficiently small as to be negligible.

PHYSICAL REVIEW VOLUME 146, NUMBER 1 3 JUNE 1966

Spin-Lattice Interaction in Ruby Measured by Electron Spin Resonance in Uniaxially Stressed Crystals*

R. B. HEMPHILL,† P. L. DONOHO, AND E. D. MCDONALD‡
William Marsh Rice University, Houston, Texas
(Received 28 January 1966)

The spin-lattice Hamiltonian first proposed by Van Vleck to explain electronic spin-lattice relaxation has been experimentally determined for Cr^{3+} ions in ruby single crystals. Its magnitude was obtained through measurements on the effect of applied uniaxial stress on the ESR spectrum of the Cr^{3+} ions. The spin-lattice Hamiltonian was found to be a quadratic spin operator, in agreement with Van Vleck's prediction, with no evidence for any other spin dependence. It was also determined through these measurements that the Cr^{3+} ions can be considered, for interactions with lattice modes, to occupy two inequivalent types of site in the Al_2O_3 lattice.

I. INTRODUCTION

THE spin-lattice interaction for an insulating paramagnetic crystal was first treated successfully by Van Vleck[1] in terms of an interaction Hamiltonian derived from crystal-field theory. In Van Vleck's treatment the interaction between the magnetic moment of an ion and vibrations of the crystal lattice comes about indirectly: the lattice vibrations modulate the crystal field, thereby perturbing the orbital state of the ion; spin-orbit coupling then transmits this perturbation of the orbital electronic motion to the spin of the ion. Because this interaction between the lattice vibrations and the spin of the ion is a second order process, Van Vleck found for the iron-group ions that he considered, which have strongly quenched orbital angular momentum, that the dominant part of the interaction can be expressed as an operator quadratic in the effective spin of the ion. This spin operator, the spin-lattice Hamiltonian, is also, to first order, linearly dependent on the lattice strain, and it therefore leads to the one-phonon spin-lattice relaxation which dominates relaxation processes at low temperature.

Using microwave-ultrasonic techniques Shiren and Tucker[2] verified Van Vleck's prediction of the quadratic spin dependence of the spin-lattice Hamiltonian, and they determined the magnitude of the interaction for several iron-group ions.[3,4] It was shown by Shiren[5] and by Donoho[6] that one-phonon relaxation times predicted from experimentally measured values of Van Vleck's spin-lattice Hamiltonian are in good agreement with observed relaxation times. An excellent review of experimental and theoretical work on spin-lattice interactions for iron-group ions has recently been published by Tucker.[7]

This paper describes a measurement of the spin-lattice Hamiltonian for Cr^{3+} ions in ruby. In this experiment uniaxial stress was applied to single crystals of

* Supported by National Aeronautics and Space Administration.
† Now at Texas Instruments, Inc., Dallas, Texas.
‡ Now at Texaco, Inc., Houston, Texas.
[1] J. H. Van Vleck, Phys. Rev. **57**, 426 (1940).
[2] N. S. Shiren and E. B. Tucker, Phys. Rev. Letters **6**, 105 (1961).
[3] N. S. Shiren, Bull. Am. Phys. Soc. **7**, 29 (1962).
[4] E. B. Tucker, Phys. Rev. Letters **6**, 183 (1962).
[5] N. S. Shiren, in *Magnetic and Electric Resonance and Relaxation*, edited by J. Smidt (Interscience Publishers, Inc., New York, 1963).
[6] P. L. Donoho, Phys. Rev. **133**, A1080 (1964).
[7] E. B. Tucker, Proc. IEEE **53**, 1547 (1965).